Please cite the Published Version

Moutevelis, Dionysios, Paspatis, Alexandros, Cheah Mañe, Marc and Gomis-Bellmunt, Oriol (2025) Impact of DC Dynamics of Grid-Forming Converters on Transmission System Stability. In: 2025 IEEE Kiel PowerTech, 29 June 2025 - 03 July 2025, Kiel, Germany.

DOI: https://doi.org/10.1109/PowerTech59965.2025.11180308

Publisher: Institute of Electrical and Electronics Engineers (IEEE)

Version: Accepted Version

Downloaded from: https://e-space.mmu.ac.uk/641533/

Usage rights: Creative Commons: Attribution 4.0

Additional Information: This is an author accepted manuscript of an article published in 2025 IEEE Kiel PowerTech. This version is deposited with a Creative Commons Attribution 4.0 licence [https://creativecommons.org/licenses/by/4.0/]. The version of record can be found on the publisher's website.

Enquiries:

If you have questions about this document, contact openresearch@mmu.ac.uk. Please include the URL of the record in e-space. If you believe that your, or a third party's rights have been compromised through this document please see our Take Down policy (available from https://www.mmu.ac.uk/library/using-the-library/policies-and-guidelines)

Impact of DC Dynamics of Grid-Forming Converters on Transmission System Stability

Dionysios Moutevelis

CITCEA-UPC

Barcelona, Spain
dionysios.moutevelis@upc.edu

Alexandros Paspatis
Dept. of Engineering
Manchester Metropolitan University
Manchester, United Kingdom
a.paspatis@mmu.ac.uk

Marc Cheah-Mañe CITCEA-UPC Barcelona, Spain marc.cheah@upc.edu Oriol Gomis-Bellmunt CITCEA-UPC Barcelona, Spain oriol.gomis@upc.edu

Abstract—In this paper, the impact of the DC-side dynamics on the stability of grid-forming converters for transmission system applications is assessed. First, a reduced order model for the DCside dynamics of a two-stage, grid-forming converter is adapted within a small-signal stability analysis framework. This reduced model captures the essential dynamics of the DC-side, achieving sufficient accuracy but without excessive computation cost for system-level studies. Then, the DC-side model is interfaced with a standard AC-side, small-signal model of a droop-controlled gridforming converter. The combined linear model of the converter is deployed for assessing relevant parameter stability limits in a case study based on a variation of the well-known WSCC transmission system. The study shows that neglecting the DCside dynamics and considering an ideal DC voltage source, leads to overly optimistic stability limits for the AC-side parameters. The validity of the proposed linear model and of the calculated parameter stability limits are supported by non-linear EMT simulations performed in Matlab/Simulink environment.

Index Terms—Inverter-based resources, Grid-forming converters, Transmission system stability, DC dynamics

I. INTRODUCTION

Power system dynamics have been altered by the massive integration of inverter-based resources (IBRs). This is particularly evident within the concept of inverter-based power systems, where IBRs are the sole generating units, therefore being responsible for the various stability functions, e.g., voltage and frequency regulation [1]. These functions are usually implemented through the control concept of Grid-Forming (GFM) inverters, which are inverters equipped with suitable control systems that are able to provide a voltage reference angle and magnitude, allowing the operation of the network independently of the presence, or lack thereof, of conventional synchronous machines [2].

Various works have aimed to investigate stability of inverter-based power systems. Early works focused on microgrids and distribution system applications [1]. Recently, transmission system-level studies have gained significant interest [3, 4], partly due to the increasing number of converter-based, generation plants that are directly connect to the transmission system level [5]. In order to investigate power system stability in either case, common approaches include small-signal and large-signal analysis [6]. As the latter is usually either based on computationally intensive Electromagnetic Transient (EMT) simulations or difficult to apply nonlinear analysis frameworks,

small-signal stability analysis corresponds to the most widely employed tool [7]. Nevertheless, when performing systemlevel small-signal stability studies, multiple assumptions are considered in order to simplify the modelling.

Among the key assumptions of previous small-signal analyses of inverter-based power systems, DC-side dynamics are often ignored, assuming a constant DC voltage source at the input of the IBR, thereby reducing the model under consideration [8]. These dynamics however can be critical when evaluating closed-loop system stability, particularly since they contain control and power system states with timescale similar to those of the states at the AC-side. For example, it was pointed out in [9] that the limitations from the converter DC-side can lead to reduced inertia provision in GFM control setups. Additionally, when the same AC/DC converter is responsible for regulating both the AC and DC voltage, possible interactions between the synchronization to the AC network and the DC-link voltage regulation may arise [10]. For this reason, dedicated DC/DC converters are frequently used to regulate the DC voltage and decouple the AC- and DC-sides of the converter [11]. However, the impact of these converters and their control loops on the transmission system stability remains unclear.

Recently, an approach aimed at simplifying the DC-side modelling of IBRs equipped with DC/DC converters, while at the same time considering the essential dynamics was proposed in [12]. This study only considered a single generation unit, corresponding however to a promising approach in investigating system-level stability properties.

In this paper, the equivalent modelling of the DC dynamics of GFM converters for photovoltaic and battery energy storage systems from [12] is leveraged. Building on those equivalent models, the impact of DC dynamics of GFM from all main technologies on transmission system stability is investigated through an elaborate small-signal stability analysis framework. The performed analysis reveals that neglecting the DC-side dynamics leads to falsely optimistic parameter stability regions, even for the cases where these parameters are related to AC-side components. The analytical conclusions are verified through EMT simulation results.

The paper is organized as follows. The DC-side dynamics model of [12] and its derivation is briefly described in

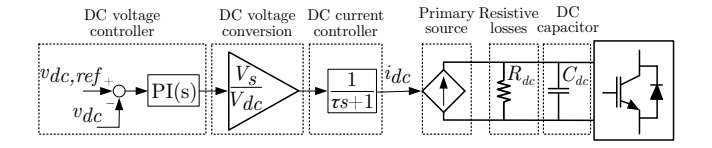


Fig. 1. Schematic of the DC-side dynamics model.

Section II while in Section III, it is adapted for small-signal stability analysis. Section IV presents a stability analysis of a representative transmission system with 100% converter based generation while including the effect of the converter DC-side dynamics, while Section V validates the proposed analysis with detailed EMT simulations. Finally, Section VI summarizes the study and offers suggestions for future work.

II. SIMPLIFIED REPRESENTATION OF DC DYNAMICS FOR NETWORK STUDIES

The model of the DC-side dynamics of GFM converters is considered in this work to assess their impact on transmission system stability and hence, its structure is reviewed in this section. Fig. 1 shows a schematic of the DC-side dynamic model, whose components are explained in the following.

In terms of electrical elements, the model includes a controllable current source, a shunt resistance, and a capacitor. The current source and the capacitor represent the primary source of the converter and the DC-link, respectively, while the resistor models the DC/DC converter losses. The losses and the value of the shunt resistor R_{dc} are calculated based on the efficiency of the DC/DC converter as in [12]:

$$\eta = \frac{P_{out}}{P_{in}}, \quad R_{dc} = \frac{V_{dc}^2}{(1 - \eta) \cdot P_{in}},$$
(1)

where η is the efficiency, V_{dc} is the nominal DC-link voltage based on the converter design and P_{in} , P_{out} are the input and output power of the device, respectively.

The control elements of the current source are selected so that they represent the operation of the DC/DC converter stage, which would control the DC-side voltage in practical applications. They include a DC-link voltage controller, a DC voltage conversion stage (V_s/V_{dc}) in Fig. 1 represents the scaling from the primary source rated voltage to the DC-link rated voltage) and a first-order transfer function. The latter two condense the voltage step-up stage, typically found in photovoltaic plants, and the dynamic response of the inner current controller of the DC/DC converter. Specifically, the current control-to-output DC current transfer function H(s) is given by [12]:

$$H(s) = \frac{-I_L K_{pi} s^2 + \left(\frac{V_{dc}}{L_{dc}} D' K_{pi} - I_L K_{ii}\right) s + \frac{V_{dc}}{L_{dc}} D' K_{ii}}{s^2 + \frac{V_{dc}}{L_{dc}} K_{pi} s + \frac{V_{dc}}{L_{dc}} K_{ii}},$$
(2)

where L_{dc} is the DC-side inductance and I_L is the steady-state inductor current. D'=1-D, where D is the duty cycle, and K_{pi} , K_{ii} , are the gains of the PI based current controller. By analyzing transfer function (2), it is revealed that one zero-pole pair (z_1, p_1) is located at low frequencies and close to zero,

thus canceling each other out. Hence, the system is mainly influenced by the remaining zero-pole pair (z_2, p_2) , leading to an approximation G(s) of H(s). Therefore, the time constant τ of the low-pass filter can be designed based on the frequency response of that pole as:

$$H(s) \approx G(s) = A \frac{1}{\left(\frac{s}{\omega_0} + 1\right)} = \frac{V_s}{V_{dc}} \frac{1}{\left(\frac{s}{K_{pi} \cdot \frac{V_{dc}}{L_{fc}}} + 1\right)}$$
(3)

where $A=H(0)=1-D=V_s/V_{dc}$ is the voltage conversion gain and $\omega_0=1/\tau=p_2\approx K_{pi}V_{dc}/L_{dc}$ is the cut-off frequency. For an in-depth version of the above analysis, the reader is referred to [12]. The modelling approach presented in this section balances simplicity and accuracy, making it suitable for system-level studies that are considered in this paper.

III. STATE SPACE MODELLING OF DC DYNAMICS FOR SMALL-SIGNAL STABILITY ASSESSMENT

In this section, the dynamic model of the GFM DC-side from [12], shown in Fig. 1, will be adapted for state space, small-signal analysis. The power balance in the DC capacitor can be written as [13]:

$$P_s = P_R + P_C + P_{ac}$$

$$\Rightarrow v_{dc}i_{dc} = \frac{v_{dc}^2}{R_{dc}} + C_{dc}\dot{v}_{dc}v_{dc} + P_{ac},$$
(4)

where P_R are the resistive losses, P_C is the power stored in the DC capacitor, $P_{ac}=3/2(v_di_d+v_qi_q)$ is the active power injected to the AC-side and P_s is the power provided by the primary source. By solving (4) for \dot{v}_{dc} , the state equation for the DC voltage is derived:

$$\dot{v}_{dc} = \frac{1}{C_{dc}} (i_{dc} - \frac{v_{dc}}{R_{dc}} - \frac{P_{ac}}{v_{dc}})
= \frac{1}{C_{dc}} (i_{dc} - \frac{v_{dc}}{R_{dc}} - \frac{3}{2} \frac{v_d i_d + v_q i_q}{v_{dc}}).$$
(5)

It should be noted that the electrical variables from the AC-side, i.e., current and voltage components i_d , i_q , v_d , v_q , respectively, expressed in a rotating dq-reference frame, as well as P_{ac} are determined by the control of the VSC-interface as well as by the grid dynamics. Their analytic description lies outside of the scope of this paper, but their modelling equations for GFM and Grid-Following (GFL) converters can be found in [1, 13].

The derivation of the analytical model for i_{dc} is detailed in the remaining of this section. By transforming the dynamics of the DC-stage conversion of (3) from the Laplace to the time domain, i_{dc} can be written as:

$$\dot{i}_{dc} = \frac{1}{\tau} (\frac{V_s}{V_{dc}} i_{s,ref} - i_{dc}).$$
 (6)

Finally, the DC-side current reference $i_{s,ref}$ is defined by the DC-voltage control dynamics as in [13]:

$$\dot{x}_{dc} = v_{dc,ref} - v_{dc},
i_{s,ref} = K_{pv}(v_{dc,ref} - v_{dc}) + K_{iv}x_{dc},$$
(7)

where $v_{dc,ref}$ is the DC-voltage reference, x_{dc} is the internal state of the DC-voltage PI controller and K_{pv} , K_{iv} are the proportional and integral gains of this PI controller, respectively. Equations (5), (6) and (7) fully define the dynamic model of the DC-side. One should note that only equation (5) contains a nonlinear term with respect to the state variables of the DC-side: $x_{dc} = [v_{dc} \ i_{dc} \ x_{dc}]^{\mathsf{T}}$, as well as of the AC-side: $x_{ac} = [v_d \ v_q \ i_d \ i_q]^{\mathsf{T}}$. By linearising (5), the state equation that is used for the small-signal analysis becomes:

$$\Delta \dot{v}_{dc} = \frac{1}{C_{dc}} \left(\Delta i_{dc} + \left(\frac{3}{2} \frac{v_{d0} i_{d0} + v_{q0} i_{q0}}{v_{dc0}^2} - \frac{1}{R_{dc}} \right) \Delta v_{dc} - \frac{3i_{d0}}{2v_{dc0}} \Delta v_d - \frac{3i_{q0}}{2v_{dc0}} \Delta v_q - \frac{3v_{d0}}{2v_{dc0}} \Delta i_d - \frac{3v_{q0}}{2v_{dc0}} \Delta i_q \right),$$
(8)

where Δ stands for small-signal perturbation and the index 0 signifies the variable values at the linearization point. Equations (6), (7) and (8) form the complete model for the DC-side dynamics. The coefficients from these equations are used to calculate the state space matrices that are used in the following section for the small-signal stability analysis.

TABLE I DC-SIDE PARAMETERS

	a 1 1	** 1
Parameter	Symbol	Value
DC capacitor	C_{dc}	5.58 pu
DC resistor	R_{dc}	14.3 pu
DC-side delay	au	0.5 ms
Proportional gain	K_{pv}	20.54
Integral gain	K_{iv}	16.35
Voltage ratio	V_s/V_{dc}	0.56

TABLE II AC-SIDE PARAMETERS

Parameter	Symbol	Value
Transformer	R_t, X_t	0.002, 0.1 pu
impedance		
Filter	R_f, X_f	0.005, 0.15 pu
impedance		
Filter	B_f	0.15 pu
susceptance		
Current controller	K_{pi}^{ac}, K_{ii}^{ac}	0.48, 5
PI gains		
Voltage controller	K_{pv}^{ac}, K_{iv}^{ac}	7.64, 6.11
PI gains		
Active/Reactive power	m_p, m_q	0.05, 0.067
droop gains		
Active/Reactive power	T_p, T_q	0.1, 0.1 s
time constants		
Measurement delay	T_d	0.1 ms

IV. SMALL-SIGNAL STABILITY ANALYSIS

In order to illustrate how the DC-side dynamics can influence the transmission system stability, a case study based on a modified version of the well-known, WSCC system is presented in this section. For the scope of this work, the stability

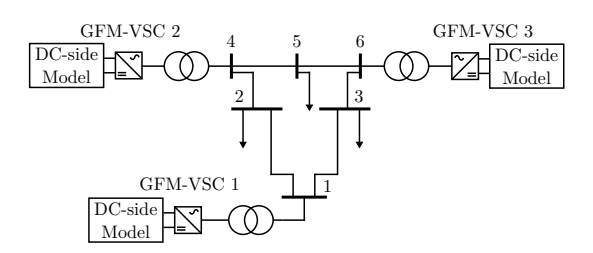


Fig. 2. Single-line diagram of the modified WSCC system.

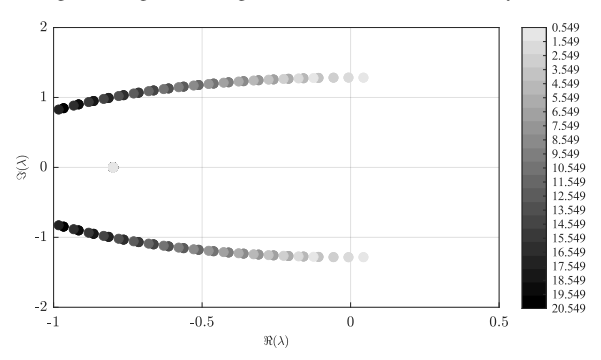


Fig. 3. Trajectories of the eigenvalues for variation of the DC-side proportional gain K_{pv} for all system converters.

of the system will be evaluated by monitoring the eigenvalues of the linear model of the complete system, including both DCand AC-side dynamics, during parameter variations. For this study, all three synchronous generators found in the original system were substituted with GFM, converter-based generation units. For all three converters, their DC-side was modelled using the equations described in Section III, while their ACside hardware and droop-based control were modelled as in [1]. A detailed schematic of both the hardware and control configurations of the converters AC-side can be found in [14]. For all cases, unless specified otherwise, the parameters of the DC-side can be found in Table I, while of the AC-side can be found in Table II. The DC-side parameters were rescaled based on the per-unit values found in [12], while the AC-side hardware parameters were selected based on typical values found in the literature [1]. The AC-side control parameters for the inner loops (voltage and current), were selected based on the modulus optimum criterion [15], while the droop gains were selected based on steady-state frequency and voltage support requirements [1, 16]. The linear model of the complete system was obtained by combining the linear models of each participating device, which were in turn analytically derived. This combination was implemented in Matlab environment by using the designated Control Systems Toolbox.

A. DC-side Parameters

First, eigenvalue sensitivity analysis was performed for variations of the DC-side parameters. For each case, these parameters were changed simultaneously for all system converters. Fig. 3 shows the eigenvalue trajectories for a reduction of the proportional gain of the DC-side voltage controller K_{pv} . This reduction, corresponding to a slower control of the DC voltage, renders the system unstable for a gain value

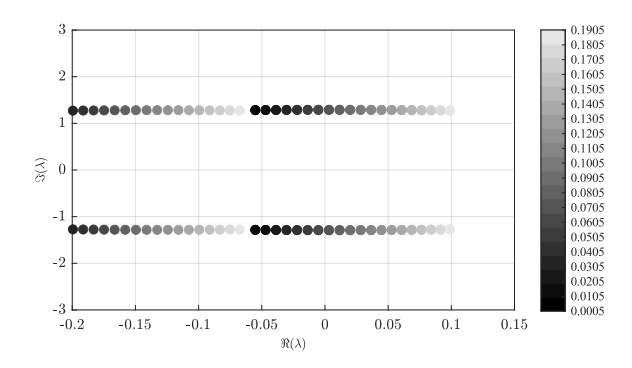


Fig. 4. Trajectories of the eigenvalues for variation of the DC-side delay au for all system converters.

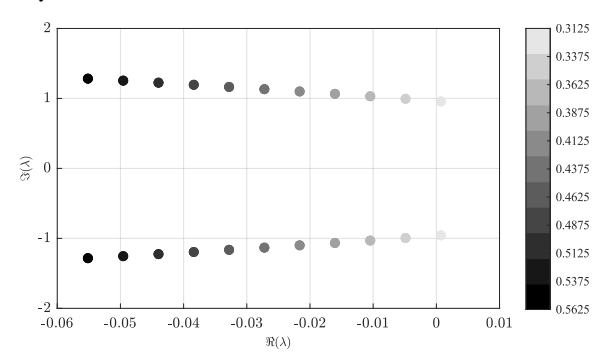


Fig. 5. Trajectories of the eigenvalues for variation of the DC-side voltage ratio V_s/V_{dc} for all system converters.

smaller than approximately 1.5. This instability highlights the necessity for the correct tuning of the DC voltage regulating controller.

Fig. 4 shows the eigenvalues trajectories for an increase in the DC-side delay parameter $\tau = L_{dc}/(K_{pi}V_{dc})$, defined in Section II. It can be seen that the instability occurs for an approximate delay value of 0.07 s, corresponding to a two orders of magnitude increase compared to the original delay value of 0.5 ms. This implies that the variation of this parameter within the range found in practical applications (typically from a fraction of a millisecond, up to a few milliseconds [12]) is not critical for maintaining system-wide stability. Finally, Fig. 5 shows the variation of the system eigenvalues for different DC-side voltage conversion ratios. For this case, the instability occurs for a ratio of approximately 0.31, representing a 44% decrease compared to the original value.

B. AC-side Parameters

Following the identification of critical parameters on the DC-side, this section highlights how their poor selection can threaten the overall system stability when combined with variations of the AC-side parameters. For the following cases, the proportional gain of the DC-side voltage controller for all system converters was set to K_{pv} =2.5. Since the parameter variations considered in this section affect the active power flow in the AC network, the linearization for the linear model calculation was repeated for each operation point. To highlight the importance of including the DC-side dynamics, even for

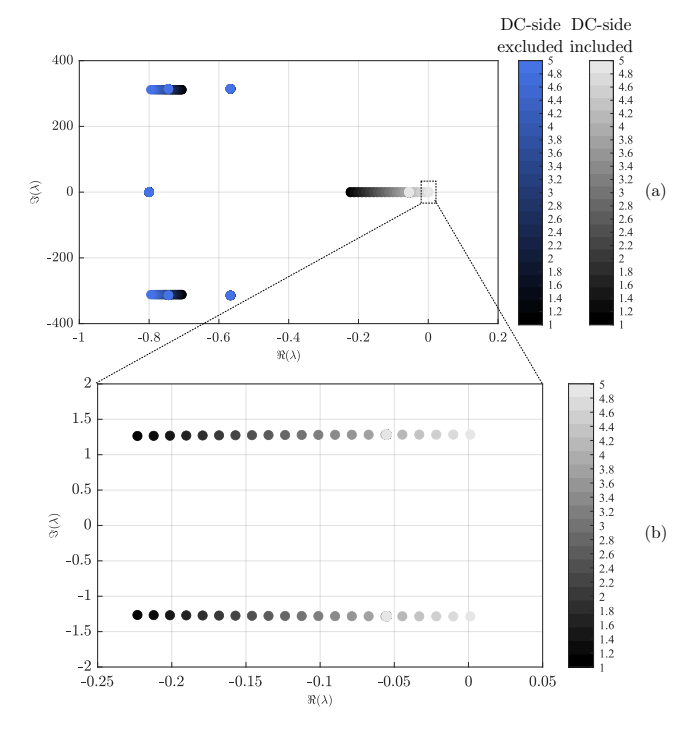


Fig. 6. Trajectories of the eigenvalues for variation of the AC-side system loading. Comparison between ideal DC voltage source model and the DC-side model of Section III. (a) Full and (b) zoomed-in version.

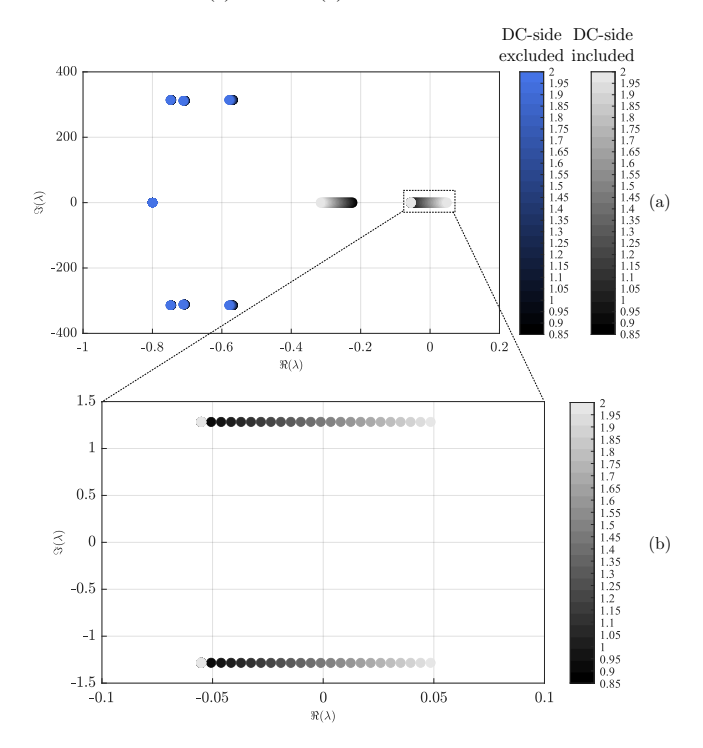


Fig. 7. Trajectories of the eigenvalues for variation of the active power reference of VSC 3. Comparison between ideal DC voltage source model and the DC-side model of Section III. (a) Full and (b) zoomed-in version.

the variation of AC-side parameters, the stability analysis was repeated for the DC-side modelling described in Section III, as well as for an ideal DC voltage source.

Fig. 6 shows the system eigenvalues for a proportional

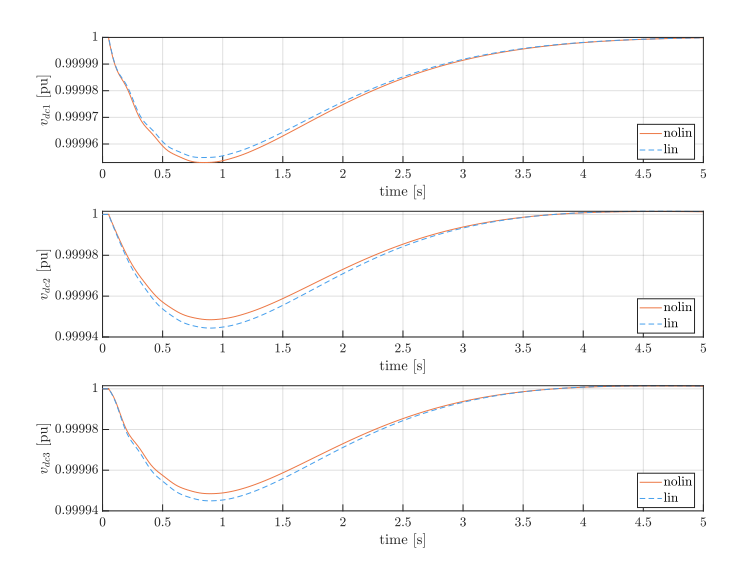


Fig. 8. Comparison of the time response of the linear and nonlinear models for a 1% load disturbance. DC-side voltage for GFM-VSC 1, 2 and 3.

increase of all system loads (shown in Fig. 2) from their original values of 0.25, 0.18 and 0.2, respectively. It can be seen that a pair of complex conjugate eigenvalues cross the imaginary axis, thus turning the system unstable, for an approximate five times increase from the original loading. At the same time, for an ideal DC source model, these eigenvalues are not present and thus, the system remains stable for the full parameter range. Fig. 7 shows the system eigenvalues for the variation of the active power reference signal of VSC 3. Similar to the previous case, the variation of the active power flow in the AC network renders the system unstable for a reference value of approximately 1.45 pu, while for the ideal DC voltage source, the system remains stable. These two examples showcase that under specific conditions, the DCside dynamics of the VSC generators can render the system unstable even if the perturbed AC-side parameters are located in a remote bus, justifying their inclusion in the study.

V. SIMULATION VERIFICATION

In this section, the stability analysis of Section IV is validated by comparing the dynamic response in the time domain of the linear model, used for the stability analysis, and a detailed nonlinear model, implemented by using Simulink and its SimPowerSystems toolbox. Additionally, the predicted parameter stability limits for two cases of Section IV are validated by applying a perturbation in the same nonlinear model.

A. Base Case

The validity of the linear model is first verified against the nonlinear model for the base, stable case, defined by the parameters of Table I and II. At $t=0.5\,$ s, a 1% load step is performed for the load connected to bus 2, as shown in Fig. 2. Fig. 8 and Fig. 9 show the comparison between the time response of the linear and nonlinear models during the disturbance and for the DC- and AC-side voltage components,

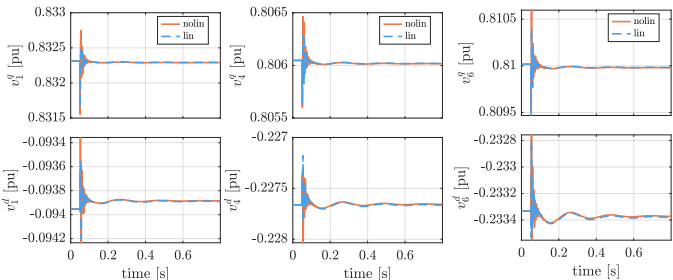


Fig. 9. Comparison of the time response of the linear and nonlinear models for a 1% load disturbance. AC-side voltage components for GFM-VSC 1, 2 and 3, connected at buses 1, 4 and 6, respectively.

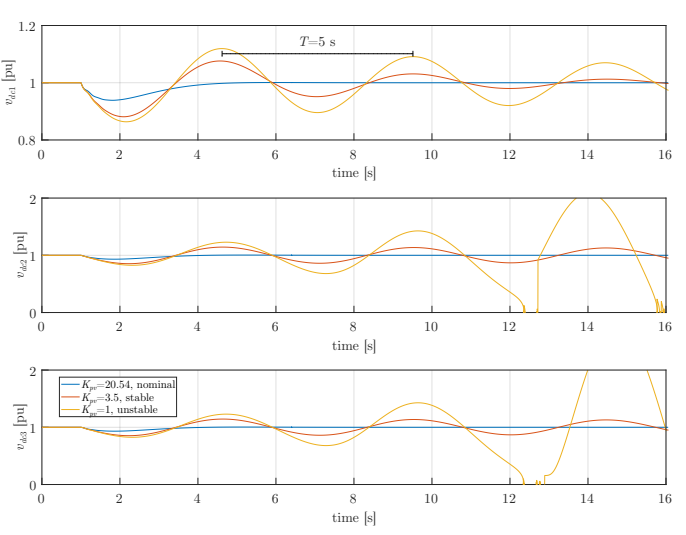


Fig. 10. Time domain validation of the parameter stability limit of the DC-side proportional gain K_{pv} . DC-side voltage for GFM-VSC 1, 2 and 3 for a 5% load step increase at t=1 s and for different gain values.

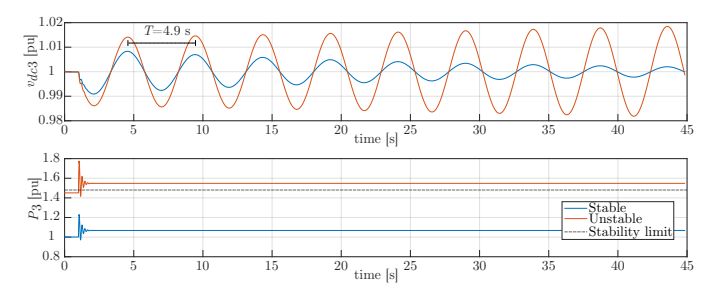


Fig. 11. Time domain validation of the parameter stability limit of the active power reference of VSC 3. DC-side voltage and active power injection for GFM-VSC 3 for a 10% active power reference increase at $t=1\,\mathrm{s}$, and for different original active power set-points.

respectively. It can be seen that the time responses match well, with accuracy up to 10^{-5} , verifying the suitability of the linear model for stability analysis.

B. Parameter Stability Limit Validation

This section validates the parameter stability margins for two cases, as predicted by the linear analysis of Section IV, by means of nonlinear, time domain simulations. The selected cases refer to the variation of the DC-side proportional gain for all system converters (Fig. 3) and of the active power reference of VSC 3 (Fig. 7).

Fig. 10 shows the DC-side voltages of the three GFM converters for a 5% load step increase, occurring at t=1 s, and for different values of the DC-side proportional gain K_{pv} . It can be seen that for the nominal value ($K_{pv}=20.54$), the transient is well-damped. For a gain value slightly larger than the critical value of 1.5 ($K_{pv}=3.5$), the voltage transient is poorly damped, but stable, while for a gain value smaller than the critical value ($K_{pv}=1$), the system becomes unstable. Additionally, the time constant of 5 s for the observed oscillation matches with the imaginary part of the unstable eigenvalues of Fig. 3 (corresponding to approximately 1.28 rad/s).

Fig. 11 shows the DC-side voltage and the active power output of VSC 3 for a 10% increase of the active power. Two different original operation set-points were considered before the step increase, one in the stable region and another one close to the critical instability value. It can be seen that when the active power injection of the converter increases past the predicted critical value of 1.45, oscillations with growing amplitude appear in the waveform of the DC-side voltage. The oscillation period of 4.9 s is in agreement with the imaginary parts of the unstable eigenvalues of Fig. 7 (approximately 1.285 rad/s). On the contrary, for the case that is well-within the predicted stable region, the oscillations in the DC-side decrease in magnitude, indicating a stable operation.

VI. CONCLUSIONS

In this paper, a reduced order, representative model for the DC-side of GFM converters is adapted for small-signal stability analysis studies. The model contains only the essential information of the DC-side dynamic states, allowing its straightforward incorporation to standard converter models for system-wide studies of transmission systems. The proposed combined model was used for the stability analysis of a representative transmission system based on the WSCC benchmark, where all conventional generation was substituted by converter-interfaced generators.

Through eigenvalue parametric sensitivity analysis, it is shown that the gains of the DC-side voltage controller have a relevant effect on the converter stability. Without their proper tuning, variations of the AC-side parameters, e.g., system loading, can render the system unstable, with oscillations of increasing magnitude and in a frequency range of around 50 Hz appearing in the DC-side voltage of the converters. By comparing the eigenvalue trajectories, it is shown that these effects are neglected when the DC-side is represented by an ideal voltage source, leading to a falsely optimistic parameter stability limit assessment. The validity of the linear analysis was supported by nonlinear, EMT simulations performed in Matlab/Simulink. Future work will focus on integrating DCside current, power and energy limitations in the proposed stability analysis framework, as well as on expanding the considered model to wind turbine plants.

ACKNOWLEDGMENTS

This publication is part of the R&D project CET Wind Digipower (PCI2023-145953-2), which is funded by the "Ministerio de Ciencia, Innovación y Universidades de España", the "Agencia Estatal de Investigación" and the European Union. The work of M. Cheah-Mañe is partially funded by the Serra Hunter Programme. O. Gomis-Bellmunt is an ICREA Academic Researcher.

REFERENCES

- [1] N. Pogaku, M. Prodanovic, and T. C. Green, "Modeling, analysis and testing of autonomous operation of an inverter-based microgrid," *IEEE Trans. on Pow. El.*, vol. 22, no. 2, pp. 613–625, 2007.
- [2] R. Rosso, X. Wang, M. Liserre, X. Lu, and S. Engelken, "Grid-forming converters: Control approaches, grid-synchronization, and future trends—a review," *IEEE Open Jour. of Ind. Ap.*, vol. 2, pp. 93–109, 2021.
- [3] I. Alvarez-Fernandez, D. Ramasubramanian, W. Sun, A. Gaikwad, J. C. Boemer, S. Kerr, and D. Haughton, "Impact analysis of ders on bulk power system stability through the parameterization of aggregated der_a model for real feeders," *El. Pow. Sys. Research*, vol. 189, p. 106822, 2020.
- [4] Y. Lin, G.-S. Seo, S. Vijayshankar, B. Johnson, and S. Dhople, "Impact of increased inverter-based resources on power system small-signal stability," in 2021 IEEE PESGM, 2021, pp. 01–05.
- [5] R. A. Khan, F. Akter, S. Khaled, M. P. Akter, and K. R. Ullah, "Design of grid forming inverter for integration of large-scale wind farm in weak grid," in 2022 4th STI Conference, 2022, pp. 1–6.
- [6] N. Hatziargyriou, J. Milanovic, C. Rahmann, V. Ajjarapu, C. Canizares, I. Erlich, D. Hill, I. Hiskens, I. Kamwa, B. Pal, P. Pourbeik, J. Sanchez-Gasca, A. Stankovic, T. Van Cutsem, V. Vittal, and C. Vournas, "Definition and classification of power system stability revisited & extended," *IEEE Trans. on Pow. Sys.*, vol. 36, no. 4, pp. 3271–3281, 2021.
- [7] Q. Chen, S. Bu, and C. Y. Chung, "Small-signal stability criteria in power electronics-dominated power systems: A comparative review," *Journal of Modern Pow. Sys. and Clean Energy*, vol. 12, no. 4, pp. 1003–1018, 2024.
- [8] A. Paspatis, G. Konstantopoulos, and S. Dedeoglu, "Control design and small-signal stability analysis of inverter-based microgrids with inherent current limitation under extreme load conditions," El. Pow. Sys. Research, vol. 193, p. 106929, 2021.
- [9] J. Girona-Badia, V. A. Lacerda, E. Prieto-Araujo, and O. Gomis-Bellmunt, "Limitations on the virtual inertia provision from grid-forming-connected renewable energy sources," *IET Conference Proceedings*, vol. 2023, pp. 166–173, 2023.
- [10] —, "Enhancing the ac network stability with a grid-forming control for single-stage pv inverter," El. Pow. Sys. Research, vol. 235, p. 110666, 2024
- [11] B. Pawar, E. I. Batzelis, S. Chakrabarti, and B. C. Pal, "Grid-forming control for solar pv systems with power reserves," *IEEE Trans. on Sus. En.*, vol. 12, no. 4, pp. 1947–1959, 2021.
- [12] X. Luo, A. G. Paspatis, A. K. Singh, N. Hatziargyriou, and E. I. Batzelis, "Modeling of dc-side dynamics in pv/battery grid-forming inverter systems," in 2023 IEEE PESGM. IEEE, 2023, pp. 1–5.
- [13] D. Moutevelis, J. Roldán-Pérez, M. Prodanovic, and S. Sanchez-Acevedo, "Bifurcation analysis of active electrical distribution networks considering load tap changers and power converter capacity limits," *IEEE Trans. on Pow. El.*, vol. 37, no. 6, pp. 7230–7246, 2022.
- [14] O. Alican, D. Moutevelis, J. Arevalo-Soler, C. Collados-Rodriguez, J. Amorós, O. Gomis-Bellmunt, M. Cheah-Mane, and E. Prieto-Araujo, "A dynamic similarity index for assessing voltage source behaviour in power systems," arXiv preprint arXiv:2501.16167, 2025.
- [15] V. A. Lacerda, E. P. Araujo, M. Cheah-Mañe, and O. Gomis-Bellmunt, "Phasor modeling approaches and simulation guidelines of voltage-source converters in grid-integration studies," *IEEE Access*, vol. 10, pp. 51 826–51 838, 2022.
- [16] D. Moutevelis, J. Roldán-Pérez, P. Rodríguez-Ortega, and M. Prodanović, "Virtual synchronous machine design for islanded microgrids using the extended impedance criterion with grid frequency dynamics included," *IEEE Trans. on En. Conv.*, 2024.